BMC Cancer

RESEARCH

Open Access

Senescence-specific molecular subtypes stratify the hallmarks of the tumor microenvironment and guide precision medicine in bladder cancer

Luzhe Yan[1,2,3,4,5†], Haisu Liang[1,2,3,4,5†], Tiezheng Qi[1,2,3,4,5], Dingshan Deng[1,2,3,5], Jinhui Liu[1,2,3,5], Yunbo He[1,2,3,5], Jinbo Chen[1,2,3,5], Benyi Fan[1,2,3,5], Yiyan Yao[4], Kun Wang[4], Xiongbing Zu[1,2,3,5,6], Minfeng Chen[1,2,3,5], Yuanqing Dai[1,2,3,5*] and Jiao Hu[1,2,3,5*]

Abstract

Background Bladder cancer (BLCA) is notably associated with advanced age, characterized by its high incidence and mortality among the elderly. Despite promising advancements in models that amalgamate molecular subtypes with treatment and prognostic outcomes, the considerable heterogeneity in BLCA poses challenges to their universal applicability. Consequently, there is an urgent need to develop a new molecular subtyping system focusing on a critical clinical feature of BLCA: senescence.

Methods Utilizing unsupervised clustering on the Cancer Genome Atlas Program (TCGA)-BLCA cohort, we crafted a senescence-associated molecular classification and precision quantification system (Senescore). This method underwent systematic validation against established molecular subtypes, treatment strategies, clinical outcomes, the immune tumor microenvironment (TME), relevance to immune checkpoints, and identification of potential therapeutic targets.

Results External validations were conducted using the Xiangya cohort, IMvigor210 cohort, and meta-cohort, with multiplex immunofluorescence confirming the correlation between Senescore, immune infiltration, and cellular senescence. Notably, patients categorized within higher Senescore group were predisposed to the basal subtype, showcased augmented immune infiltration, harbored elevated driver gene mutations, and exhibited increased senescence-associated secretory phenotype (SASP) factors expression in the transcriptome. Despite poorer prognoses, these patients revealed greater responsiveness to immunotherapy and neoadjuvant chemotherapy.

Conclusions Our molecular subtyping and Senescore, informed by age-related clinical features, accurately depict age-associated biological traits and its clinical application potential in BLCA. Moreover, this personalized assessment framework is poised to identify senolysis targets unique to BLCA, furthering the integration of aging research into therapeutic strategies.

†Luzhe Yan and Haisu Liang contributed equally to this work.

*Correspondence:
Yuanqing Dai
dycooper@126.com
Jiao Hu
hujiao@csu.edu.cn
Full list of author information is available at the end of the article

Keywords Bladder cancer, Cellular senescence, Tumor microenvironment, Molecular subtype, Precision medicine

Introduction

Bladder cancer (BLCA) is the 10th most prevalent carcinoma with high incidence and mortality among urinary malignancies worldwide, leading to substantial societal burden [1]. For individuals, the high heterogeneity of the BLCA tumor microenvironment (TME), which consists of various types of cells and cellular matrices, contributes to diverse clinical outcomes, most of which are unfavourable [2]. The unsatisfactory clinical outcomes specifically suggest that traditional regimens for BLCA, centered around radical cystectomy and cisplatin-based chemotherapy, have encountered a bottleneck in terms of limited efficacy and prognosis [1]. Recent advancements have introduced neoadjuvant chemotherapy and immunotherapy for BLCA. However, personalized assessment has lacked comprehensive integration of genomics with clinical data for precise treatment selection and efficacy evaluation [1, 3]. Therefore, we are dedicated to the development of new molecular stratification tools and quantitative systems to facilitate precision medicine for BLCA [4]. From the perspective of tumor evolution, it takes an average of 10–15 years for the normal urothelium to progress from being cytologically normal to developing oncogene mutations and then to advanced or metastatic urothelial carcinoma [1, 5]. This implies that tumor diversity is not static but rather constitutes a dynamic, four-dimensional process that unfolds across both spatial and temporal dimensions.

Age functions as a quantifiable metric of accumulated risk, encompassing exposure events and genetic mutations over time in clinical contexts, particularly in BLCA [6, 7]. The National Institute of Health (NIH) reported in the SEER (Surveillance, Epidemiology, and End Results Program) data that the average age at diagnosis and death for BLCA patients was over 70 years old in the United States. More notably, a majority of BLCA patients are diagnosed at an age exceeding 65 years, and the mortality rate increases with advancing age [6, 7]. Indeed, aging reshapes the somatic landscape of tumor patients [8], leading older individuals to exhibit higher oncogenic burden of mutations compared to younger ones [9]. Therefore, BLCA is often perceived as a geriatric disease [6]. At the cellular level, the biological processes of aging and carcinogenesis are inherently incompatible [10, 11]. However, at the sample level, considering mutual time-dependent effects, aging and malignancy actually share various mechanisms, referred to as meta-hallmarks. The interplay between these commonalities constitutes the basis for the dual role of aging in promoting and inhibiting tumors [10]. Besides meta-hallmarks, paradoxical characteristics unique to aging, namely giant cell autophagy and cellular senescence, are gradually being recognized to hold great potential as breakthroughs in addressing cancer [10].

Moreover, an advanced age associated with BLCA suggests an ageing TME [12]. In the BLCA TME, fibroblasts and immune cells are particularly susceptible to aging-related changes, leading to the secretion of the senescence-associated secretory phenotype(SASP) factors [13]. This results in a cascade of aging effects that significantly influence the overall TME response to various treatments [14]. Currently, senescence-related therapies, including senolytics and senomorphic drugs, have demonstrated significant potential across a variety of cancers. Emerging evidence has systematically characterized the senescent tumor microenvironment in hepatocellular carcinoma (HCC) and prostate adenocarcinoma, revealing age-related cellular reprogramming that promotes therapeutic resistance [15, 16]. Parallel investigations in bladder cancer have shifted focus toward delineating immune-modulatory stromal subpopulations, particularly their spatial distribution patterns and functional crosstalk in patients receiving immune checkpoint inhibitors [17]. However, the effects of aging on the TME and anti-tumor immunity have not been comprehensively studied in BLCA.

To establish a foundation for additional research in this field, we investigated the role of senescence-related genes in the BLCA TME, confirming the critical influence of aging on the anti-tumor immunity cycle. Here, we introduce a novel classification system based on age-related characteristics in BLCA, followed by the introduction of a quantitative scoring system, termed the Senescore. The Senescore is designed to evaluate individual TME status and immune potential, offering insights for precise BLCA treatment and prognosis evaluation.

Materials and methods

Data preparation and preprocessing

Xiangya transcriptome cohort

This cohort, rigorously collected and sequenced independently by Xiangya Hospital, includes 57 bladder cancer (BLCA) samples and 13 normal bladder tissues to generate mRNA sequencing profiles, as detailed in our previous studies [18–21]. The Xiangya cohort has been deposited in the Gene Expression Omnibus (GEO) database under accession number GSE1887155 [22].

Xiangya tissue microarray (TMA) cohorts

The TMA dataset consists of 50 untreated BLCA samples and 51 BLCA samples treated with immune checkpoint inhibitors [21, 23, 24].

The Cancer Genome Atlas (TCGA) cohort-BLCA.

TCGA-BLCA cohort, containing transcriptome profile with clinical annotations of 400 BLCA patients, was originally downloaded from the website UCSC Xena. With initial data cleaning and normalization, we straightly captured three forms showing RNA-seq of encoding genes only, namely counts, FPKM and TPM. Mutation profile, especially the copy number variation(CNV) was processed with GISTIC2.0 [25]. Tumor mutation burden (TMB) is further computed with VarScan2.

IMvigor210, the BLCA Immunotherapy cohort

IMvigor210 is a clinical immunotherapy trial, blocking PD-L1 with atezolizumab, on BLCA patients inappropriate for cisplatin therapy [26]. We extracted and curated the consolidated RNA-seq matrix with clinical annotations from the study by Mariathasan S et. al [27].

Gene Expression Omnibus (GEO) cohorts

GSE48075 is a transcriptome dataset for BLCA [28], while GSE32894 pertains to urothelium carcinoma [29]. Both datasets were retrieved from the GEO database. We employed the "sva" R package to merge these two datasets into a meta-dataset.

Filtering BLCA specific senescence-related genes and unsupervised clustering

We comprehensively collected all genes which could potentially correlate with aging of BLCA patients. Three ways collectively contribute to the original gene list, named as Raw_Gene_Set. Firstly, we extensively collected genes from the portal MSigDB mainly in terms of two features of ageing specific to cancer, namely autophagy and cellular senescence. Otherwise in GenAge portal [30], packed human lifespan-related genes were included. In OPEN GENES [31], we collected genes related to various topics including "Changes in gene activity affect the age-related process", "Senescence" and "Regulation of genes associated with aging". Secondly, we acquired tissue-specific genes from various sources. In CellAge portal [32], cell type was restricted to BLCA. In AgeAnno [33], differentially expressed genes(DEGs) between the old and middle-aged bladder samples were captured. In Digital Ageing Atlas (DAA), tissue type was restricted to bladder. Thirdly, we referred to latest publications to avoid ignoring genes that databases, somehow, excluded due to timeliness [34]. We finally pooled all genes derived from different sources and the Raw_Gene_Set containing 3115 genes was constructed. For the record, all genes included were taken from researches on ageing or lifespan of Homo Sapiens.

Next, in TCGA-BLCA cohort, we performed differential analysis on expression matrix of Raw_Gene_Set between the old (>65 y) and the middle-aged (≤65 y). Eight genes, showed potential discrepancy, which were further incorporated into Cluster_Gene_Set. This gene list contained SSTR5, BMP5, CRTAC1, WIF1, CCL11, FGF7, UCHL1 and NCAM2. We then applied Cluster_Gene_Set into unsupervised clustering under the condition: maximum evaluated k of 6, resamplings(reps) of 100, item resampling (pItem) of 0.8, gene resampling (pFeature) of 1. Kmdist clustering algorithm (clusterAlg) was partitioning around medoids (PAM) and distance was spearman. Comprehensive comparison among 6 clustering results indicated advantage of two distinct BLCA molecular subtypes, which were named as Senecluster.

Construction of the BLCA senescence quantification system: Senescore

Senescore was derived from the Senecluster. 1155 DEGs between two clusters were identified using "limma" R package. We performed univariate cox analysis to further screen DEGs with prognostic significance. Expression matrix on 318 significantly prognostic DEGs was put into principal component analysis (PCA). We considered the eigenvector of PC_1 as the coefficient matrix in the formula. Specifically, the formula writes: $\text{Senescore}_i = \sum_{k=1}^{318} \text{PC\_1}_{ik} * \text{Z\_Exp}_{ik}$,

Senescore_i is the quantitative senescore value of BLCA patient_*i*. *k* is the number of one gene, ranking from 1 to 318. For instance, *k* represents one random gene, Gene_*k*. PC_1_{ik} is the coefficient of Gene_*k*. Z_Exp_{ik} is the expression of Gene_*k* after Z-score standardization.

Classical BLCA molecular subtypes

Molecular subtype system is of potential value in clinical application, playing an important role in the diagnosis, treatment and prognosis of BLCA. As reported in previous works [19–22], seven widely proven molecular subtypes were followed by our research for further prediction and therapy indication [28, 29, 35–39].

We calculated and obtained identifications of seven molecular classifiers on individual based on RNA-seq matrix from various cohorts using R packages including "ConsensusMIBC" and "BLCAsubtyping". Combined with our constructed quantification system, we explored the potential of Senescore to predict different molecular subtypes in patients with receiver operator curve (ROC) analysis, while area under curve (AUC) was considered a measure of prediction accuracy.

Survival analysis, enrichment analysis and mutational analysis

Kaplan–Meier curve (K-M) was performed with "survival" package and visualized with "survminer" package. For enrichment analysis, single-sample gene set enrichment analysis (ssGSEA) was conducted to calculate enrichment score (ES) of selected gene set or signature at single-sample level. We used gene set variation analysis (GSVA), using "GSVA" package, to calculate ES of specific signature in a cohort. Alternatively, for RNA-seq matrix after differential analysis, gene set enrichment analysis (GSEA) was conducted. To confirm the biological functions of DEGs, we conducted Gene Ontology (GO) and Kyoto Encyclopedia of Genes and Genomes (KEGG) analyses. Differential mutation map was obtained with "maftools" package and chi-square test was used to verify the statistical significance.

Illustrating the BLCA tumor microenvironment (TME) multidimensional immune features

The analytical approach in this section aligns with that of previous studies [19–21, 24]. At molecular level, we explored the correlation between Senescore with 122 collected immunomodulators and 36 markers of 5 vital tumor-infiltrating immune cells (TIICs). At cellular level, we applied two validated methods, MCP-COUNTER and TIMER, into calculating the infiltration state of TIICs. Moreover, the activity of the TIICs, reported as the cancer immunity cycle, was evaluated with online analysis platform: TIP. We also performed enrichment analysis and revealed relevant immune pathways [40].

Prediction of treatment efficacy in BLCA patients

We identified the mutational landscape of therapeutically relevant mutant targets between binary groups divided by Senescore. We selected neoadjuvant chemotherapy (NAC) related genes including TP53, RB1, PIK3CA, ERBB2, ATM, ERCC2, BRCA1 and FANCC from the study by Giobanni M et. al [41]. For erdatinib therapy, we focused on mutation profile of two genes, namely FGFR2 and FGFR3 [42–44]. Therapeutic signatures and drugs, related to radiotherapy, target therapy and immunotherapy, were methodically gathered up previously.

Especially in immune checkpoint blockade (ICB) therapy, we first explored the correlation between the Senescore with various immunotherapy effect indicators and signatures including EMT markers, panfibroblast TGF-β reaction score, MANTIS score and T cell-inflamed score (TIS) [45]. TIS was developed within 18 genes from pan-cancer analysis and was of momentous value in predicting the clinical response to ICB treatment. We then correlated the Senescore with collected 22 immune checkpoints and potential targets listing as MYBL2 [46], SBSN [47], GATA6 [48], GATA3 [49], PTP4A3 [50], S100A5 [19], BCAT2 [21], YTHDF2 [51], PLAGL2 [52], TRIP13 [53] and Siglec15 [24] that received considerable attention and validation.

Polychromatic immunofluorescence

We employed a multi-color immunofluorescence technique to investigate the interplay between $SFRP2^+$ cells, $CD8^+$ cells and cellular senescence ($P16^+$ cells [54, 55]) at the cellular level. DAPI was used for nuclear staining [23], while specific primary and secondary antibodies were utilized for the staining of $SFRP2^+$ (Mouse: Ag18840, proteintech, USA), $P16^+$ (Rabbit: Ag1328, proteintech, USA), and $CD8^+$ (Mouse: Ag11111, proteintech, USA) cells. Initially, we examined the co-expression patterns of SFRP2, P16, and CD8 across two TME phenotypes (Inflammed and Non-inflammed), as well as their respective expression patterns. Subsequently, we compared pairwise co-expression patterns of three proteins in two immune subtypes by flow cytometry to reveal a quantified relationship between senescore, cell senescence, and CD8T cell infiltration. Moreover, we performed spatial analysis of the expression of P16 and CD8 in regions characterized by high and low SFRP2 expression.

Statistical analysis, visualization & Biostatistical criteria

All data processing, analysis and visualization was carried out in R (Version 4.2.2). *P* value of less than 0.05 was considered statistically biological significance. BLCA patients were dichotomously grouped according to the median or the best cut-off value of Senescore.

For samples fitting Gaussian distribution altogether, t-test was used to compare between binary groups. Alternatively, we use Mann–Whitney U-test to deal with samples with skewed distributions. For categorical variables, we used chi-square test to reveal significance. All statistical assumptions were consistent with biological and medical basic logic. All hypothesis tests are two-sided.

Data availability

RNA-seq data with clinical information

The data are available from the corresponding author on reasonable request.

Xiangya RNA-seq cohort, namely the GSE188715, could be captured at GEO database: https://www.ncbi.nlm.nih.gov/geo/query/acc.cgi?acc=GSE188715; GSE32894: https://www.ncbi.nlm.nih.gov/geo/query/acc.cgi?acc=GSE32894; GSE48075: https://www.ncbi.nlm.nih.gov/geo/query/acc.cgi?acc=GSE48075; TCGA-BLCA cohort: https://xenabrowser.net/; IMvigor210: http://research-pub.Gene.com/imvigor210corebiologies/;

Gene collection database

MSigDB: https://www.gsea-msigdb.org/gsea/msigdb; GenAge: https://genomics.senescence.info/genes/index.html; CellAge: https://genomics.senescence.info/cells/query.php?search= ; Digital Ageing Atlas (DAA):https://ageing-map.org/atlas/results/?sort=name&s=&species%5B%5D=9606&t=tissue; Ageanno: https://relab.xidian.edu.cn/AgeAnno/#/.

Drug database

DRUGBANK: https://go.drugbank.com/.

K-M analysis for SFRP2 expression in BLCA patients. https://kmplot.com/. [56].

Results

Age-Based Senecluster Classification via RNA Sequencing

Figure 1A provides a preliminary overview of our findings. We assembled 3115 characteristic genes, covering various aspects of BLCA aging biology, termed the Raw_Gene_Set (Table S1). We conducted a differential analysis on RNA-seq data between the younger (≤65 years old) and the elderly (>65 years old) BLCA patients, identifying eight age-specific genes to construct the Cluster_Gene_Set (Fig. 1B,Table S2). The correlation map of eight genes highlighted their prognostic implications, as elucidated by log-rank test and inter-gene associations (Fig. 1C). Using the eight genes from the Cluster_Gene_Set, we performed unsupervised classification to categorize BLCA patients into two age-related subgroups, namely Senecluster 1 ($N=257$) and Senecluster 2 ($N=143$) after comprehensive evaluation (Figure S1A-I). Subsequently, we illustrated the expression patterns of genes in Cluster_Gene_Set across the binary Seneclusters, integrated with other clinical characteristics (Fig. 1D). Patients within Senecluster1 were notably older with poor prognosis (Fig. 1E-F).

Potential clinical applications of senecluster-based senescore combined with age

Three steps facilitated the development of the Senescore based on the Senecluster (Fig. 2A). Differential analysis between the clusters primarily identified 1155 differentially expressed genes (DEGs) (Fig. 2B).

Among the screened DEGs, basal subtype-specific markers such as KRT6A and luminal subtype-specific markers including KRT20, UPK1A, and UPK2 were identified (Fig. 2B, Table S3). Senecluster showed similarities to classical BLCA subtypes, with comparable effects and potential for clinical application. From the list of DEGs, we identified 318 genes with significant prognostic value and established the Senescore using principal component analysis (PCA) (Fig. 2C). The Senescore correlates with senescence-related biological features. Gene Ontology (GO) and Kyoto Encyclopedia of Genes and Genomes (KEGG) analyses revealed the comprehensive function of Senescore (Fig. 2D-E). These results emphasized the role of extracellular matrix (ECM) in the biological foundation of crosstalk between cancer and aging. Based on the above results, we speculate that the senescence-related signature influences the ECM through various biological processes, including the PI3K-Akt pathway and structural biology, which could affect senescence or malignancy.

Patients were categorized into two groups based on the median Senescore: high Senescore and low Senescore. Survival analysis indicated difference between the two groups, and the high Senescore indicated negative prognosis (Fig. 2H). There was a correlation between Senescore and individual age to a certain extent. A scatter diagram displayed the distribution of Senescore across ages, grouped by Seneclusters (Fig. 2F). Patients in Senecluster1 were observed to have higher ages and Senescore compared to those in the other group (Fig. 2F). A statistical difference also existed between Senescore of two groups when divided by age ($p=0.0071$, Fig. 2G). When divided into four subsets by integrating age and Senescore, there was a significant survival difference observed ($p<0.001$, Fig. 2I). These results suggested the potential clinical application of combining age with Senescore to estimate the prognosis of BLCA patients.

Senescore reflected the mutation landscape

Comparing mutation profiles of the top 30 genes between low and high Senescore groups revealed varying mutation rates (Figure S2A-B). The high Senescore group exhibited higher mutation rates in TP53 (55%) and KMT2D (29%) associated with poor prognosis compared to the low Senescore group (Figure S2A-B). Abundant mutations and elevated mutation rates in crucial loci of key tumor driver genes, notably RB1 and TP53, within the high Senescore group, correlated with poor prognosis (Figure S2C-F).

Senescore indicated classical molecular subtypes and therapeutic strategies.

A high Senescore was associated with the basal subtype in Baylor, UNC, MDA, and TCGA classification system, enriched in basal differentiation, EMT differentiation, and immune differentiation, indicating poor prognosis (Fig. 3A-B). The low Senescore group showed luminal differentiation, urothelial differentiation, and Ta pathway characteristics, aligning with luminal subtype and a more favorable prognosis (Fig. 3A-B). The receiver operating characteristic (ROC) curve analysis comprehensively evaluated the sensitivity and specificity of Senescore in predicting molecular subtypes (Fig. 3C). Patients with a low Senescore were found to be more responsive to target therapies on oncogenic pathways, in contrast, those

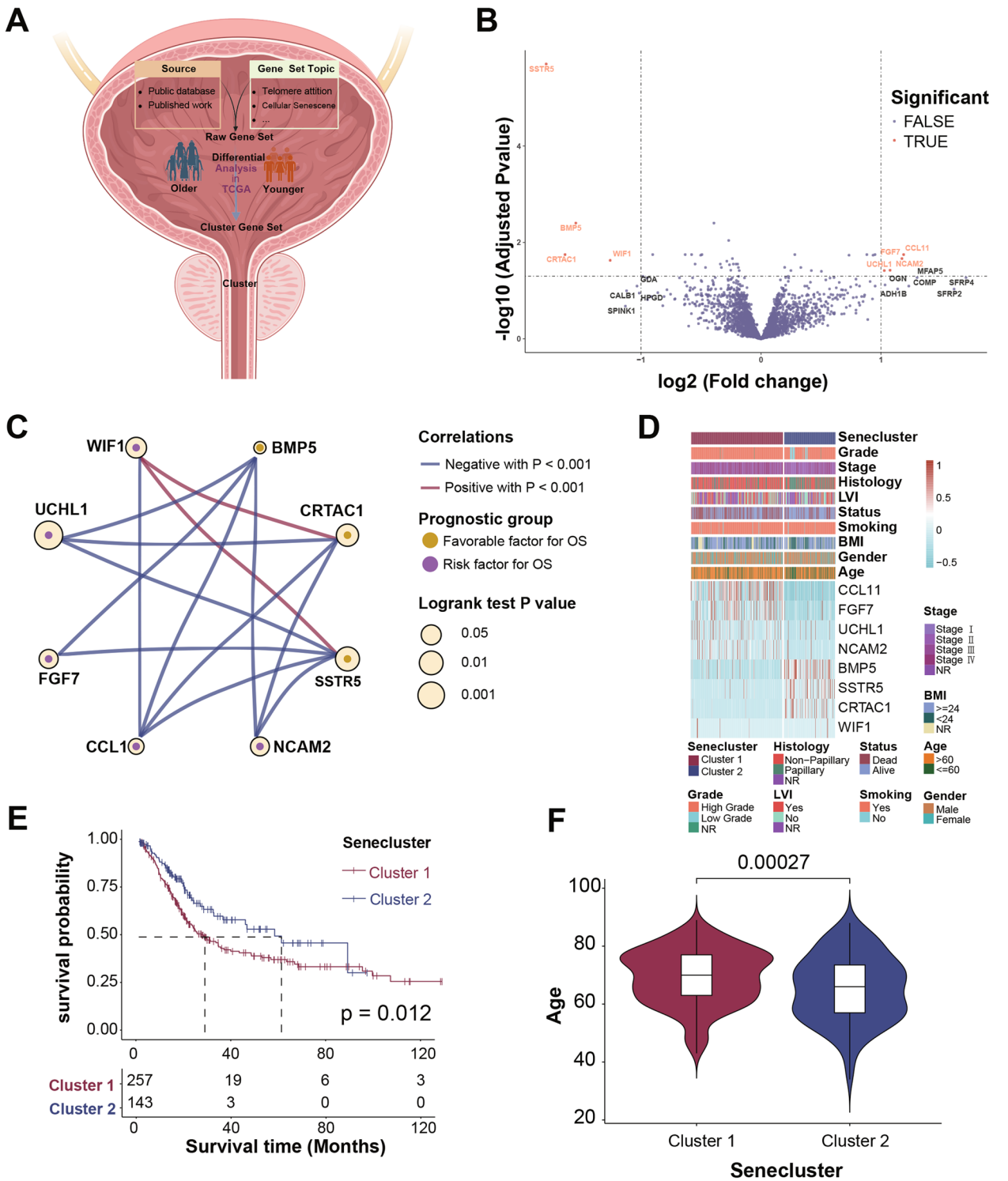

Fig. 1 Creation of Senecluster based on age by RNA sequencing. **A** Overview of path to clustering. **B** Volcano plot screening the DEGs related with ageing. **C** Correlation, prognosis, and log-rank test P-value of 8 selected genes. **D** Expression patterns of screened genes across seneclusters. **E** Kaplan–Meier curves for patient survival in Sene clusters 1 and 2. **F** Violin plot indicates ageing difference between two Seneclusters

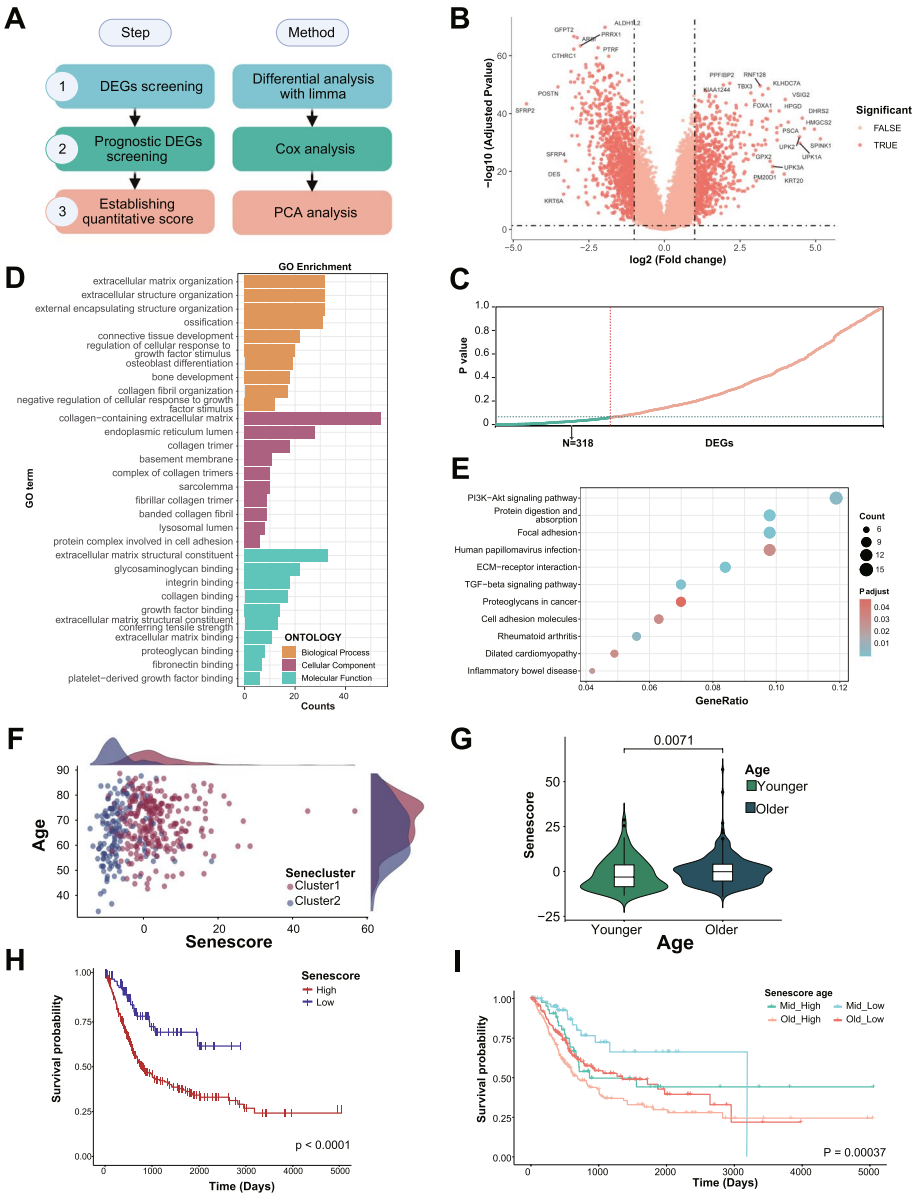

Fig. 2 Senecluster-based Senescore combined with age has potential clinical applications. **A** Path to establishing the Senescore. **B** Volcano plot showing 1155 DEGs. **C** 318 DEGs screened by prognostic value. **D** GO analysis indicated the Senescore was enriched in senescence related pathways, especially in extracellular biological processes. **E** KEGG analysis in high Senescore. **F** Scatter plot describing the relationship between age, score, and cluster. **G** Significant difference between Senescore of the middle-aged and the elderly. **H** Survival difference between high and low Senescore groups. **I** Survival differences between groups labeled with Senescore and age

with a high Senescore benefited more from epidermal growth factor receptor (EGFR) targeted therapy and radiotherapy (Fig. 3D). Specifically, patients with high Senescore demonstrated favorable responses to cetuximab, atezolizumab, and docetaxel, whereas low Senescore patients were particularly responsive to sorafenib and vinblastine (Fig. 3E).

The classical molecular subtype acted as a bridge, linking Senescore with therapeutic strategy and hinting at potential clinical decisions. Clinical benefit from neoadjuvant chemotherapy (NAC) was notably influenced by individual molecular subtype [1]. Focusing on a NAC-related gene list, we found more patients in the low Senescore group had more NAC-related gene

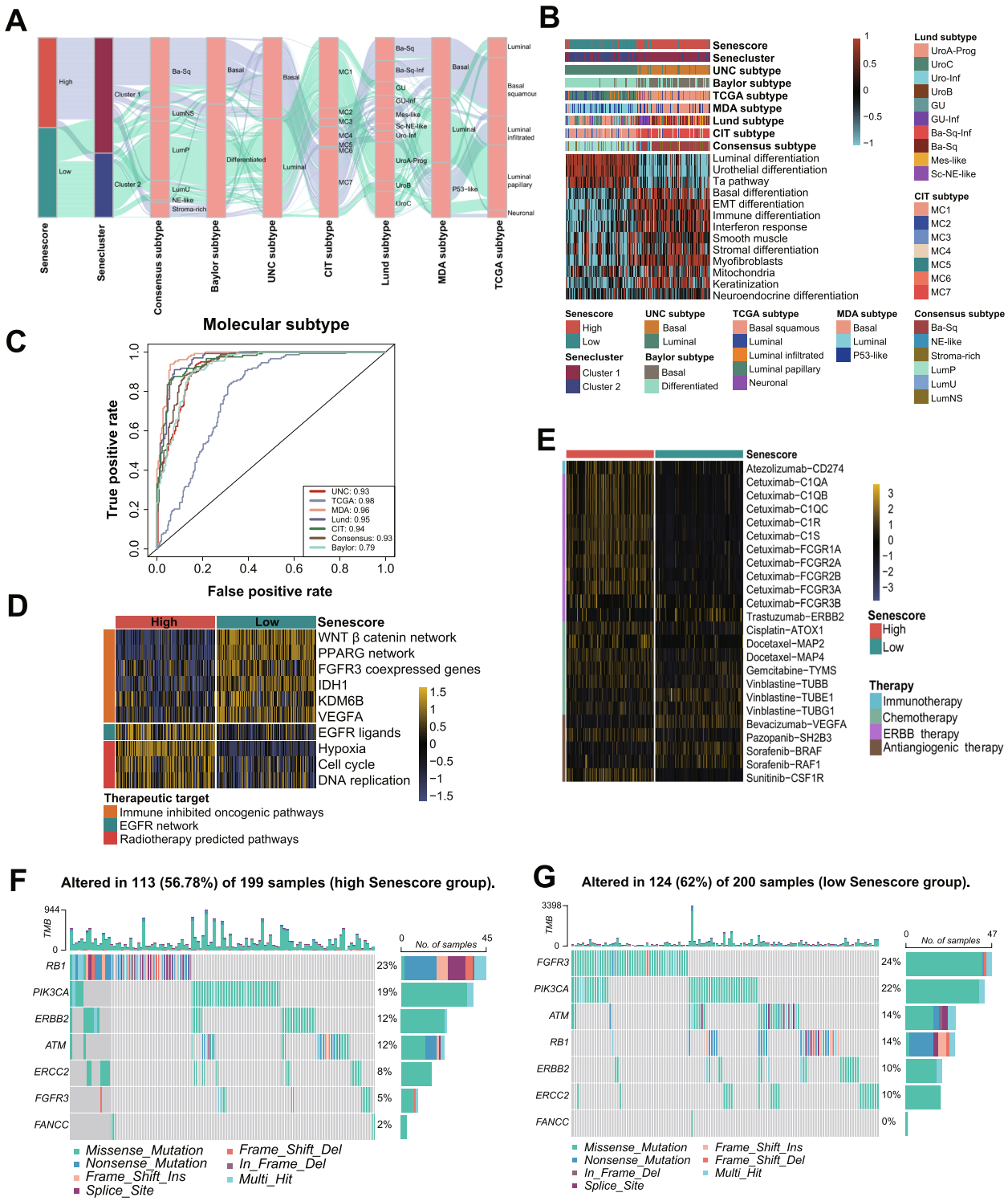

Fig. 3 Senescore indicated classical molecular subtypes and therapeutic strategies. **A** Correlation between Senescore, Senecluster and 7 classical molecular subtypes for BLCA. **B** Heatmap of pathway enrichment in Senescore and Senecluster groups labeled with seven classical molecular subtypes. **C** ROC analysis of Senescore predicting classical molecular subtypes. **D** Assessment of treatment sensitivity profiles in high and low Senescore groups. **E** High and Low Senescore groups evaluation of various drug sensitivity. **F** Mutation landscape of NAC-related genes in high Senescore group. **G** Mutation landscape of NAC-related genes in low Senescore group

mutations compared to the other group (62% vs 56.78%, Fig. 3F-G). Given recent advances in erdafitinib clinical application for BLCA, we found FGFR2/FGFR3 mutation rates higher in the low Senescore group compared to the other (Figure S3A-B).

Senescore as an effective differentiator of TME immune States

High Senescore groups showing up-regulation of immunomodulators and SASP factors (Figure S4A-B). Effector genes from key immune cells were overexpressed (Fig. 4A), suggesting higher levels of immune cell

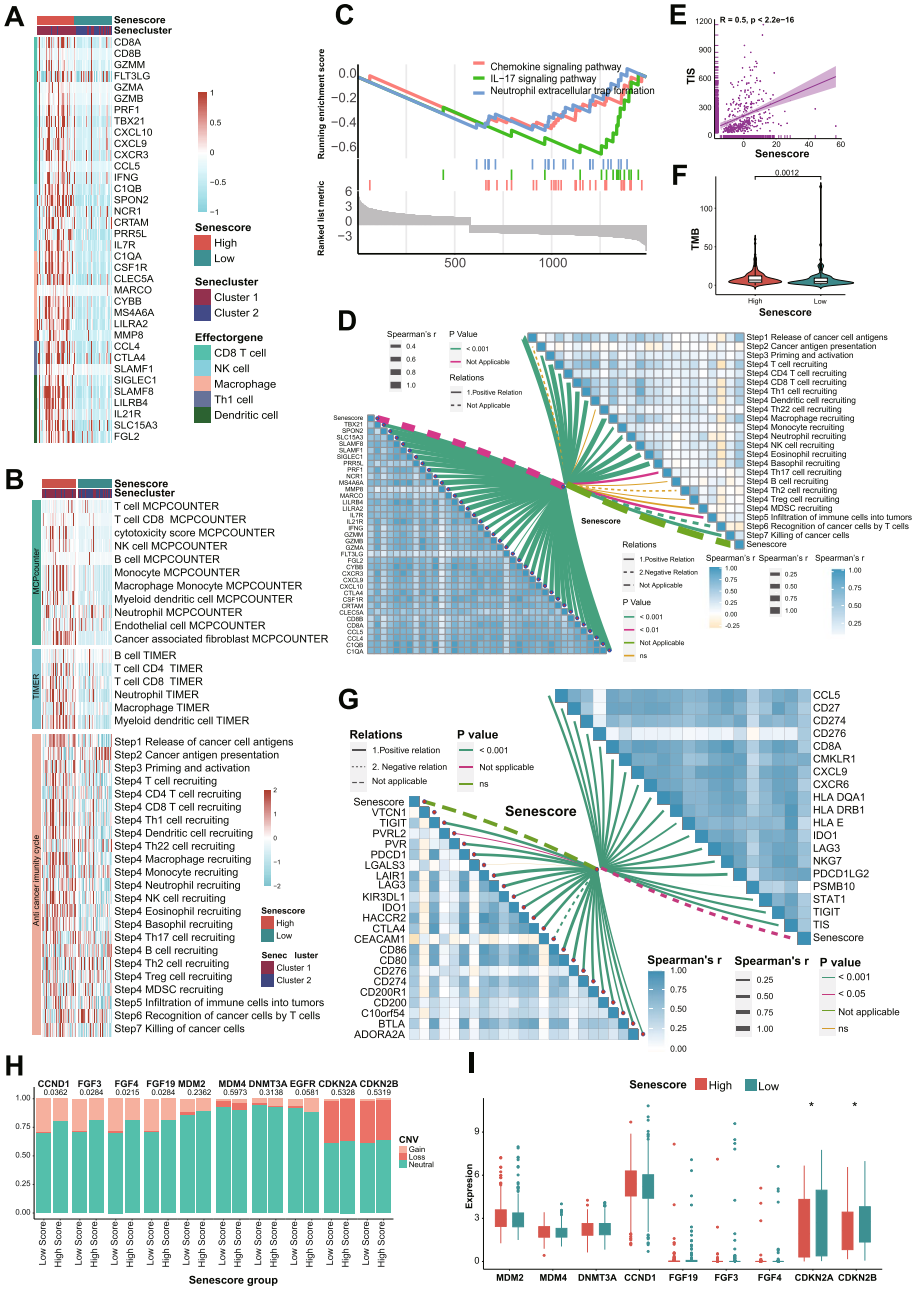

Fig. 4 Senescore effectively differentiated TME immune states. **A** Effector genes expression of five vital immune cells in Senescore and Senecluster groups. **B** Predicted levels of immune infiltration and anti-cancer immunity cycle in Senescore and Senecluster groups. **C** GSEA analysis of Senescore. **D** Correlation between Senescore with immune cell effector genes and specific steps of anti-cancer immunity cycle. **E** Linear correlation between Senescore with TIS. **F** Differential distribution of TMB in two Senescore groups. **G** Correlation between Senescore with TIS effector genes and Correlation between Senescore with immune checkpoints. **H** Mutation difference of immune hyperprogression related genes between two Senescore groups. **I** Expression of immune hyperprogression related genes between two Senescore groups

infiltration in high Senescore and Senecluster1(Fig. 4B). The high Senescore and Senecluster1 group exhibited significant immune cell population differences, consistent across MCP-COUNTER (Figure S4C-D) and TIMER (Figure S4E-F) analyses, except for neutrophils. As expected, most steps of the anti-tumor immunity cycle were activated in high Senescore and Senecluster1 (Fig. 4B). Differential activation of steps 1 to 5 between high and low Senescore groups was noted, and the outcomes within Senecluster remained consistent. (Figure S4G-H). Gene set enrichment analysis (GSEA) analysis revealed high expression of chemokine, IL-17 signaling pathways, and neutrophil extracellular trap formation in the high Senescore group (Fig. 4C), with all effector markers significantly correlating with Senescore (Fig. 4D). This correlation extends to many anti-tumor immunity cycle steps (Fig. 4D), suggesting that active pathways reflected stronger immune infiltration in high Senescore. Moreover, activated neutrophil extracellular trap formation indicated differential neutrophil expression (Fig. 4C), underscoring the comprehensive impact of Senescore on TME immunological states.

Patients with a high Senescore demonstrated enhanced T cell-inflamed score (TIS), indicating a more pronounced immune cell infiltration compared to the low Senescore group. A confirmed linear relationship between Senescore and TIS, with a slope of 0.5, underscored this correlation ($p < 0.001$, Fig. 4E). Meanwhile, the results showed a high Senescore correlated with significantly higher tumor mutation burden (TMB) ($p = 0.0012$, Fig. 4F). Most TIS key genes were concentrated in the high Senescore group (Figure S5B), with all crucial genes constructing the TIS significantly correlating with Senescore (Fig. 4G). Positive correlations between Senescore and most immune checkpoints, including PD-1, PD-L1, and CTLA-4, except for CEACAM1, were noted (Fig. 4G). The high Senescore group exhibited differential expression of BLCA validated targets (Figure S5B-C). Pathway enrichment scores, associated with immune checkpoint blockade (ICB) response, were significantly up-regulation in high Senescore group (Figure S5D). The levels of CDKN2A and CDKN2B, genes negatively associated with immune hperprogression [57], were notably reduced in the low Senescore group (Fig. 4H-I). In summary, high Senescore links to enhanced immune infiltration, suggesting potential immunotherapy benefits but also risks of immune hyperprogression and adverse outcomes, marking its significant role in predicting clinical responses to ICB.

Functional analysis and clinical implications of senescore in bldder cancer

Differential enrichments in KEGG pathways, oncogenic pathways, and metabolic hallmarks were noted across groups between age subgroups and Senescore groups. KEGG analysis confirmed 16 and 6 differentially enriched pathways between age subgroups and Senescore groups, respectively (Fig. 5A-B). Intersection of enriched pathways highlighted the role of KEGG PANTOTHENATE AND COA BIOSYNTHESIS in both aging and cancer (Fig. 5C). Repeating the operation uncovered 18 oncogenic pathways (Figure S6A-C, Table S4) and 10 metabolic hallmarks (Figure S7A-C, Table S5) clarifying the cancer-aging nexus across groups. Functionality differences between Senescore groups accounted for prognosis and treatment selection variability.

We explored the clinical application of the model. Senescore and Senecluster were linked to standard clinical traits (Fig. 5D). Age and Senescore, selected through univariate Cox regression for multivariate analysis, were chosen for bedside assessment based on their statistical significance ($p < 0.05$, Figure S5E). A nomogram, utilizing only individual age and Senescore, was then constructed to evaluate individual prognosis, demonstrating the combined potential of these factors in clinical predictive utility (Fig. 5F).

Validating of Senescore in the Xiangya cohort

In the Xiangya cohort, high Senescore was associated with basal subtypes, whereas the low Senescore group showed a preference for luminal subtypes (Fig. 6A). Specifically, significant enrichment in luminal differentiation, urothelial differentiation, and the Ta pathway characterized the low Senescore group, while the high Senescore group was marked by extracellular matrix-related pathways, including stromal differentiation and myofibroblast activation (Figure S8A). The areas under the ROC curves (AUCs) for Senescore prediction of classical molecular subtypes, ranging from 0.84 to 0.98, demonstrated high accuracy (Fig. 6C). Additionally, patients with low Senescore were sensitive to immune inhibited therapies on oncogenic pathways, whereas EGFR targeted therapy and radiotherapy were beneficial for patients with a high Senescore (Fig. 6B). The overall immune landscape delineated for the cohort revealed an inflamed TME in the high Senescore group, characterized by numerous up-regulated immunomodulators (Figure S8B). Consistently, Senescore was significantly correlated with ICB-related signatures and extensive anti-tumor immunity, indicating

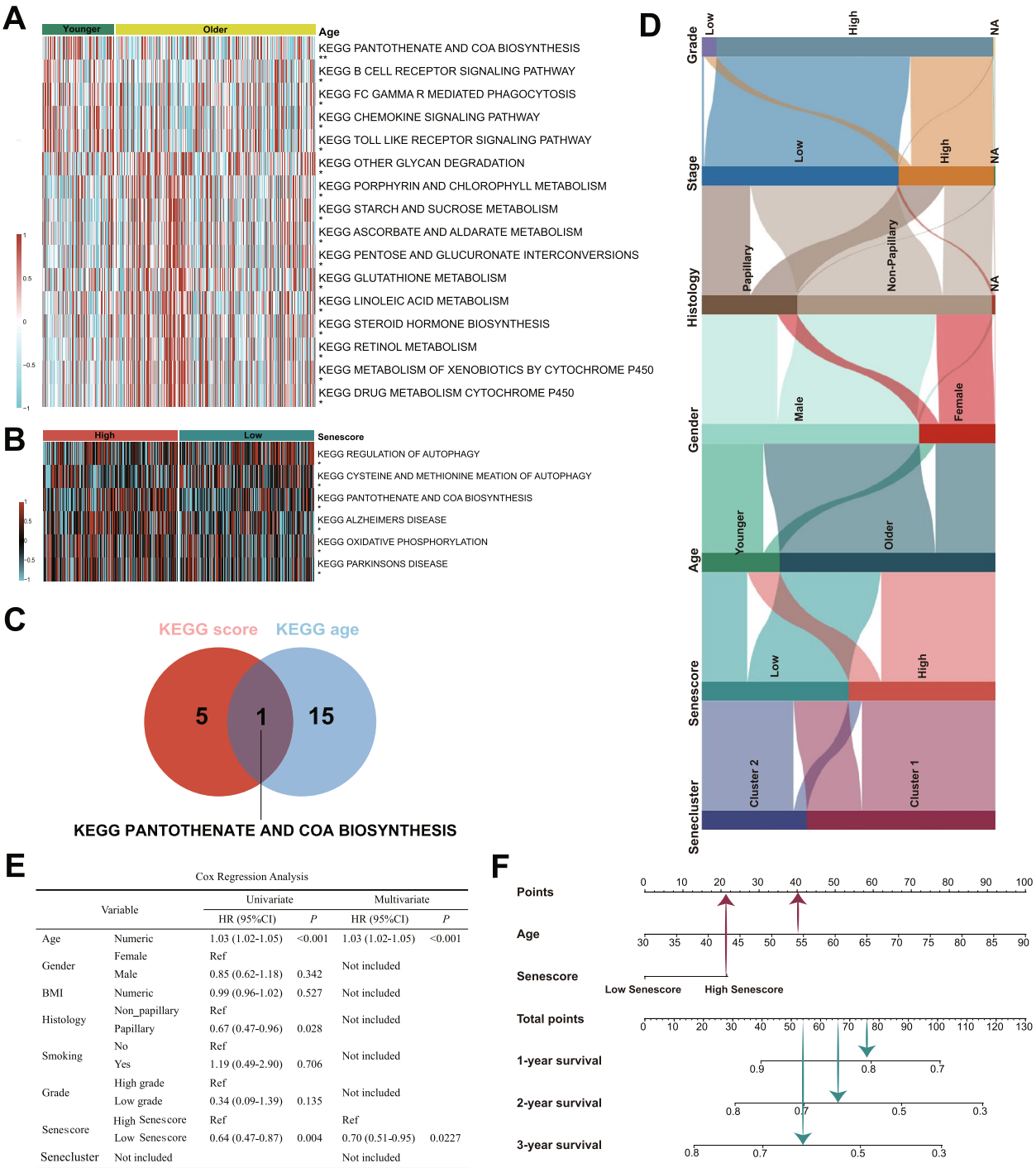

E

Cox Regression Analysis

Variable		Univariate		Multivariate	
		HR (95%CI)	*P*	HR (95%CI)	*P*
Age	Numeric	1.03 (1.02-1.05)	<0.001	1.03 (1.02-1.05)	<0.001
Gender	Female	Ref		Not included	
	Male	0.85 (0.62-1.18)	0.342		
BMI	Numeric	0.99 (0.96-1.02)	0.527	Not included	
Histology	Non_papillary	Ref		Not included	
	Papillary	0.67 (0.47-0.96)	0.028		
Smoking	No	Ref		Not included	
	Yes	1.19 (0.49-2.90)	0.706		
Grade	High grade	Ref		Not included	
	Low grade	0.34 (0.09-1.39)	0.135		
Senescore	High Senescore	Ref		Ref	
	Low Senescore	0.64 (0.47-0.87)	0.004	0.70 (0.51-0.95)	0.0227
Senecluster	Not included			Not included	

Fig. 5 Senescore-cancer links elucidated by function analysis and clinical applications of Senescore. **A**-**B** KEGG pathways differentially enriched between age (**A**) and Senescore groups (**B**). **C** Intersection of difference pathways between age groups and those between score groups. **D** Correlation between Senescore, Senecluster and clinicopathological information. **E** Conduction of univariate and multivariate cox regression on clinicopathological information. **F** Nomogram from multivariate cox regression

dense immune component infiltration in the TME within high Senescore (Fig. 6E). Furthermore, Senescore correlated with a significant number of immune checkpoints, notably PD-1, PD-L1, CTLA-4, and TIGHT (Figure S8C-G), underscoring its potential in guiding clinical decisions and understanding the TME dynamics.

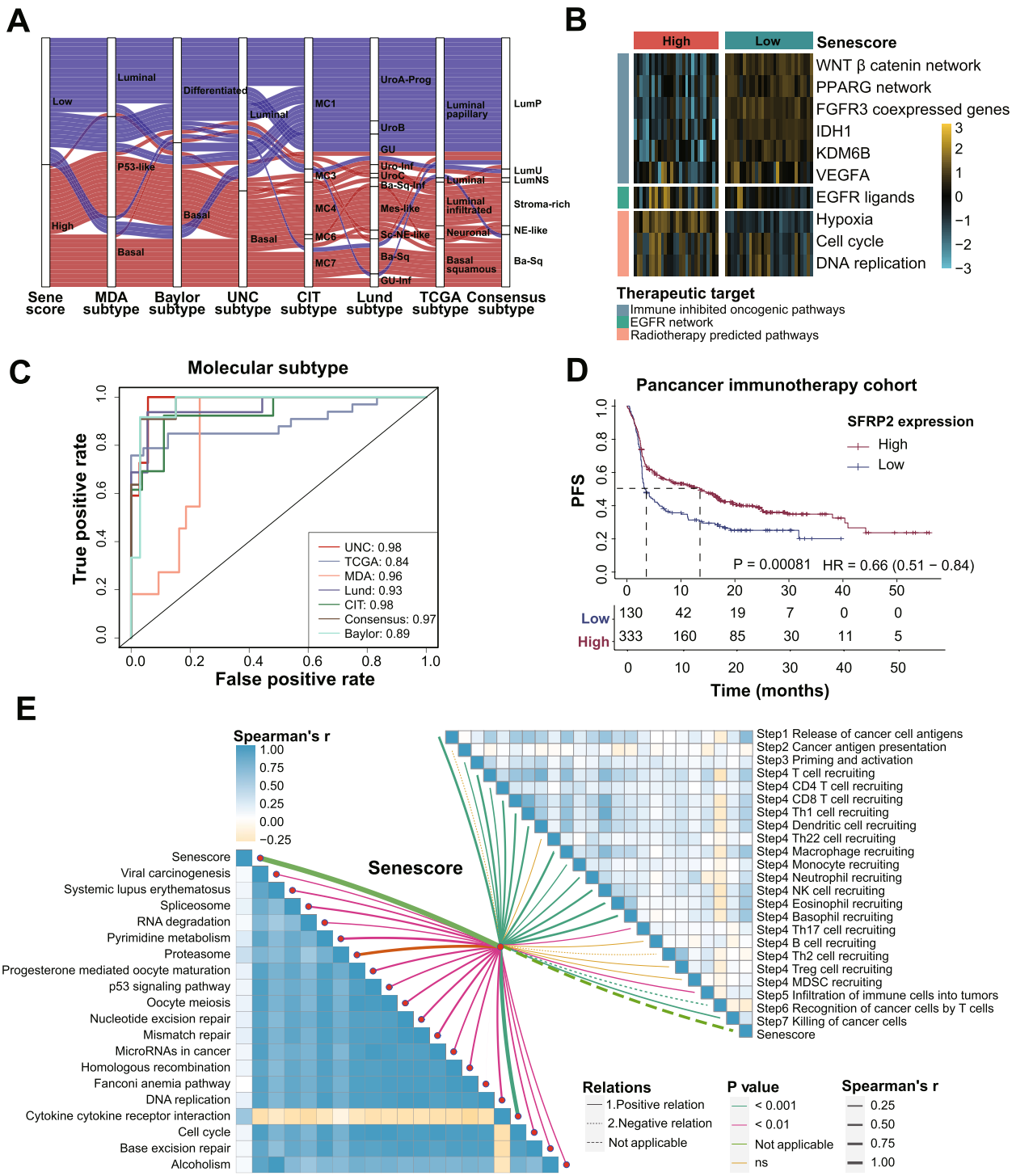

Fig. 6 Validating the role of Senescore in Xiangya cohort. **A** Correlation between Senescore and classical molecular subtypes. **B** Heatmap displays the correlation between Senescore and various target therapeutic strategies. **C** ROC analysis of Senescore predicting seven molecular subtypes in Xiangya cohort. **D** Survival difference between high- and low-SFRP2 expression patients. **E** Correlation between Senescore and positive ICB signatures

We identified SFRP2 as the most up-regulated gene in the high Senescore group and selected it as a surrogate for Senescore (Fig. 2B), facilitating verification through immunofluorescence. Additionally, P16 as classic aging marker, was selected to assess the aging state. In the Xiangya tissue microarray (TMA) cohort, we utilized multiple immunofluorescences to investigate the interplay among Senescore (SFRP2), cytotoxicity immunity (CD8), and cellular senescence (P16). Patients were categorized as 'inflamed' or 'non-inflamed' based on CD8 T cell status. High SFRP2 expression was linked to optimistic prognosis in pan-cancer immunotherapy cohort (N = 463, Fig. 6D). Tricolor maps revealed that high P16 and SFRP2 expression predominantly surrounded tumor-infiltrating CD8 T cells in inflamed patients, a pattern less evident in non-inflamed individuals (Fig. 7A). Comparatively, co-expression levels of P16/SFRP2, P16/CD8, and CD8/SFRP2 were markedly higher in inflamed than in non-inflamed patients (Fig. 7B). Gradient analysis of distances from $SFRP2^+$ cells within inflamed patients showed a decline in $P16^+$ and $CD8^+$ T cell counts from proximal to distal zones, unlike in non-inflamed patients, suggesting a spatial relationship between Senescore, T cell immunity, and cellular senescence (Fig. 7C).

Validating of Senescore in the IMvigor210 cohort and meta-cohort

In the context of the immunotherapy cohort (IMvigor210 cohort), the Senescore system underwent further validation. Initial analysis indicated an absence of discernible survival disparities between high and low Senescore groups across the entire population (Fig. 8A). However,

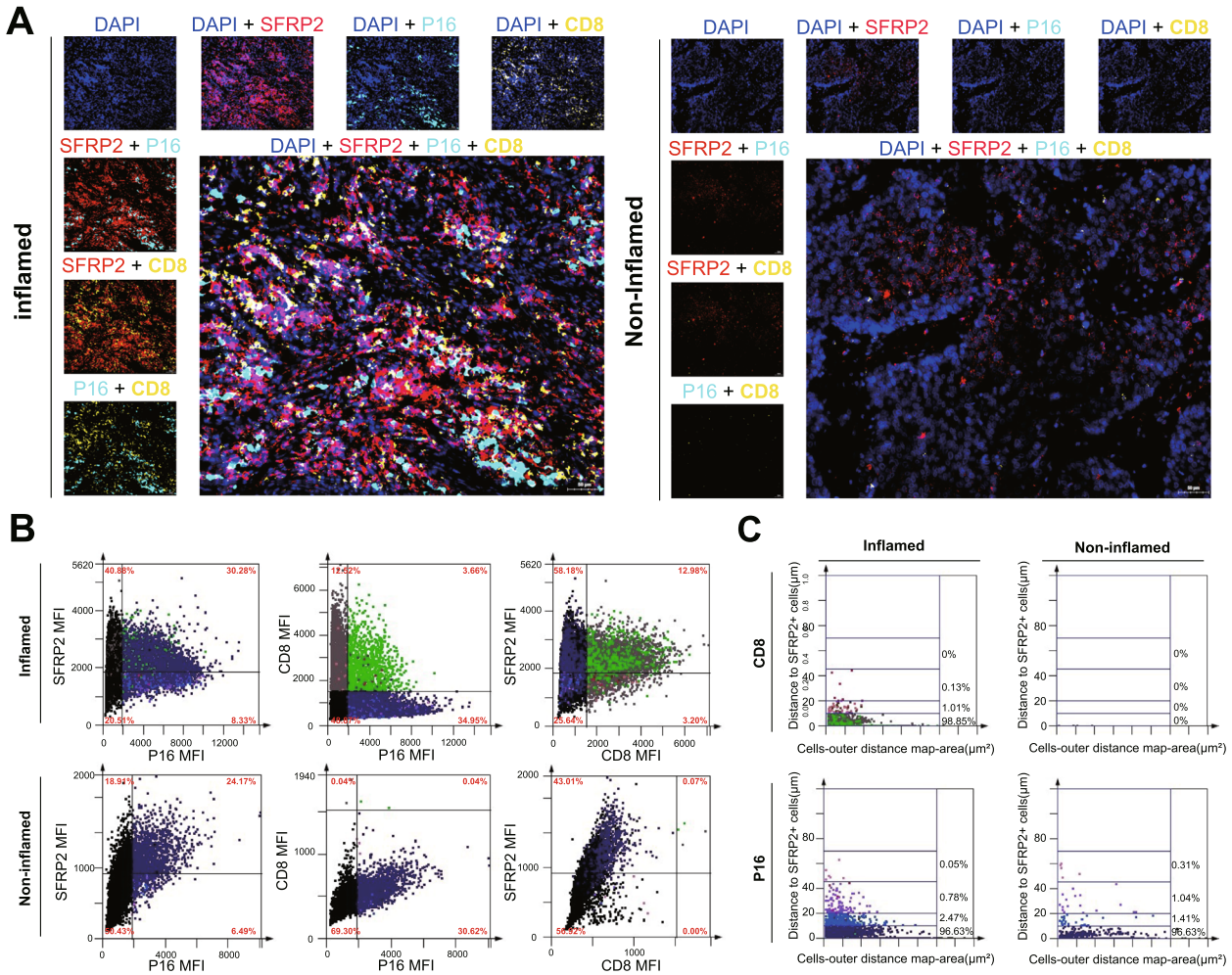

Fig. 7 Interactions between Senescore, cytotoxic Immunity and cellular senescence in Xiangya cohort. **A** Multicolor fluorescent protein co-expression map in inflamed and non-inflammed BLCA patients. **B** Co-expression of P16/SFRP2, P16/CD8, and CD8/SFRP2 in inflamed and non-inflammed BLCA patients. **C** Spatial distance gradient analysis of P16 + cells and CD8 + T cells to SFRP2 + cells

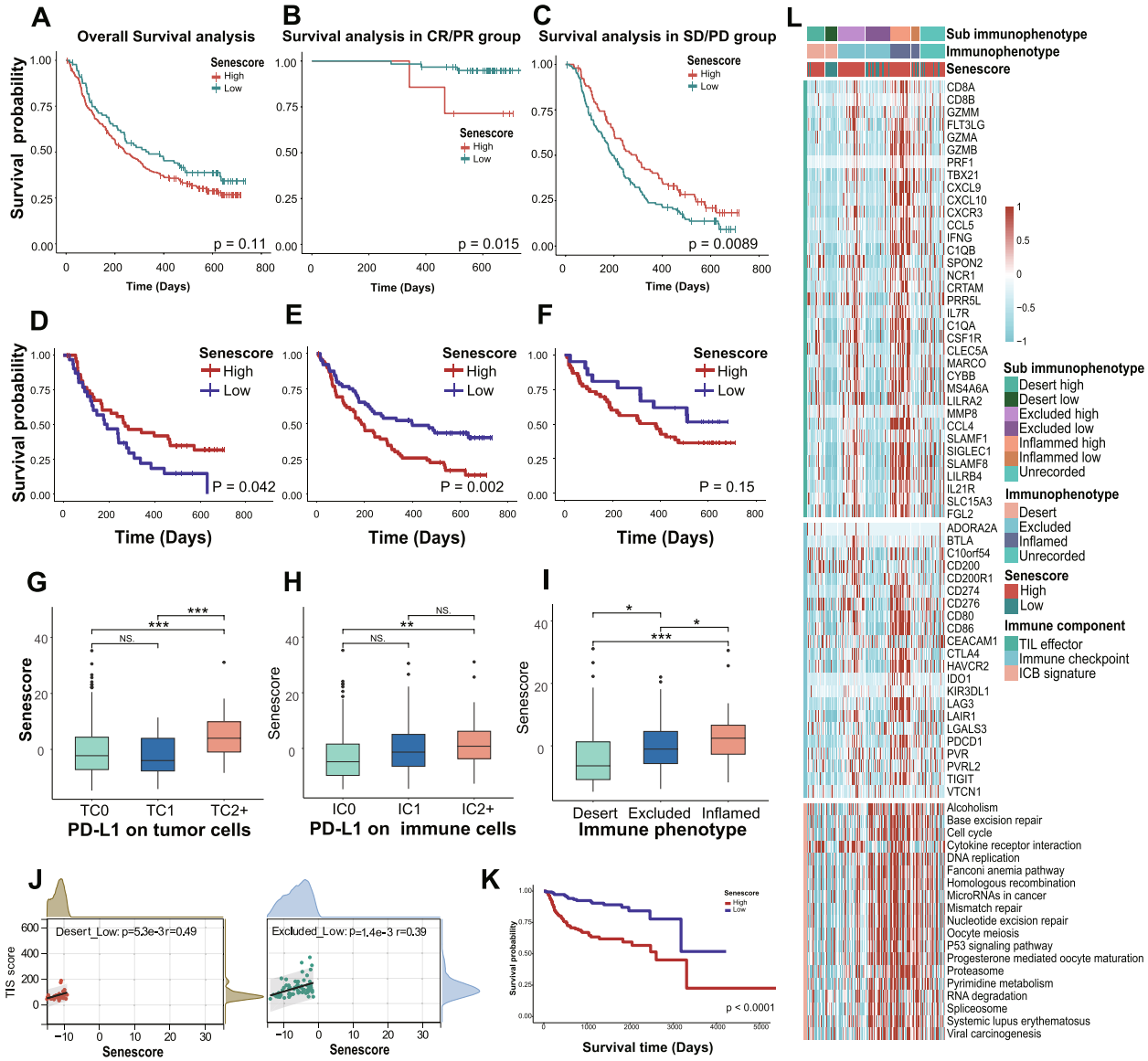

Fig. 8 Validating the role of Senescore in IMvigor210 cohort and meta-cohort. **A** Survival difference in overall Senescore group. **B** Survival difference between Senescore groups in CR/PR subset. **C** Survival difference between Senescore groups in SD/PD subset. **D** Survival analysis in desert immunophenotype. **E** Survival analysis in excluded immunophenotype. **F** Survival analysis in inflamed immunophenotype. **G** Correlations between Senescore and PD-L1 level on immune cells. **H** Correlations between Senescore and PD-L1 level on tumor cells. **I** Differences in Senescore between different immune phenotypes. **J** Linear fitting curve of the relationship between the Senescore and TIS in desert and excluded Immunophenotypes. **K** Survival difference between Senescore groups. (*$P < 0.05$; **$P < 0.01$; ***$P < 0.001$)

upon further stratification based on treatment response, intriguing patterns emerged. Low Senescore patients in the response (CR) or partial response (PR) categories exhibited better prognoses (Fig. 8B), while those with high Senescore demonstrated more favorable outcomes in the stable disease (SD) or progressive disease (PD) subsets (Fig. 8C). Considering the reinvention of immunotherapy on TME, the IMvigor210 cohort was categorized into three immune subtypes: desert, excluded, and inflamed. Furthermore, regression analysis revealed a positive linear correlation between TIS and Senescore in patients with a low Senescore within desert and excluded subtypes, suggesting the utility of Senescore as a predictive marker (Fig. 8J, Figure S9A). In the desert immune subset, high Senescore patients surprisingly had better outcomes (Fig. 8D), and those with a low Senescore more

often fell into SD/PD categories (Figure S9C). Conversely, in inflamed and excluded subtypes, respectively, the high Senescore group consistently exhibited poor prognosis, with most responders (CR/PR) having low Senescore (Fig. 8E-F, Figures S9C). We showcased the expression landscape of tumor infiltrating lymphocytes (TIL) effectors, immune checkpoints, and ICB-related signatures, observing their upregulation in high Senescore across all immune phenotypes, indicating a 'hot' TME (Fig. 8L). Interestingly, ICB-related signature enrichment was more closely associated with the inflamed immunophenotype than with Senescore levels, differing from patterns in desert or excluded subtypes (Fig. 8L). Senescore varied across different clinical feature groups (Fig. 8G-I, Figure S9B), suggesting its utility in evaluating individuals accepted immunotherapy by integrating Senescore and immune subphenotypes for clinical decisions and benefit prediction. In the meta-cohort, the high Senescore group exhibited poor prognosis, aligning with expectations (Figure S8K). Key immunomodulators and TIL markers were elevated in this group (Figures S9D-E), aligning with the Cancer Genome Atlas Program (TCGA) findings and confirming the Senescore system's robustness and adaptability.

Discussion

The exploration of aging and senescence in BLCA is pivotal, given its prevalence in the elderly, significant economic and societal impacts. With current research still nascent, the necessity for novel strategies that cater to the aging demographics of BLCA patients is clear, particularly as existing treatments often fall short for the elderly. Promisingly, advancements in age-related therapies, especially senolytics, are making strides in cancer care. The development of molecular subtyping for BLCA, based on aging traits, offers valuable insights for personalized treatment and prognosis. In this study, we introduce Senecluster, a classification derived from the aging distinctions between senile and middle-aged BLCA patients, further refined into the Senescore system for individual aging level quantification. The Senescore system employs continuous quantification to effectively overcome the limitations of binary classification, precisely characterizing the heterogeneity of BLCA and showcasing its promising potential as a clinical marker within the medical domain.

The validation of the Senescore system demonstrated robustness across multiple dimensions, notably its capacity to efficiently and accurately prognosticate survival outcomes. In the TCGA-BLCA cohort, meta-cohort, and Xiangya cohort (all excluding patients who underwent immunotherapy), lower Senescore consistently aligned with a more favorable prognosis. Conversely, among immunotherapy recipients in the IMvigor210 cohort, Senescore tailored prognosis prediction to the specific immune landscape. Notably, patients with a high Senescore within the desert immunophenotype exhibited optimistic prognostic expectations, diverging from the outcomes observed in other subgroups and the TCGA cohort. This variation underscored the impact of immunotherapy-induced spatio-temporal heterogeneity on survival, prompting a deeper exploration of the Senescore-TME relationship. In cohorts excluding immunotherapy, Senescore intricately correlated with numerous immune markers within the TME, with a high Senescore signaling an inflamed TME rich in immune regulatory factors, key immune cells, and pathways conducive to anti-tumor activity.

In BLCA, high immune infiltration does not always portend a positive prognosis. Our research elucidated that patients characterized by a high Senescore demonstrated augmented expression of SASP factors at the transcriptomic level, indicating a senescent TME conducive to tumor evolution and malignancy advancement, potentially resulting in poorer outcomes. Our study firstly uncovered the complex role of SASP factors and their relation to tumor dynamics, hinting that their presence not solely be ascribed to aging. Additionally, the relationship between Senescore with individual age is not direct; instead, it mirrored the impact of age-related gene sets, serving as a proxy for biological frailty rather than chronological age.

This study provides valuable insights but also has limitations. Firstly, incorporating additional sequencing data with survival outcomes and validation through other methods like proteomics or metabolomics could enhance the study's validity. Secondly, foundational research is crucial to understand how age-related therapies can be best utilized for BLCA treatment. In a subsequent study, we will investigate the differences in the tumor immune microenvironment between patients with high and low Senescore using multi-omics approaches. Our primary focus will be on the cellular subpopulations that contribute to variations in immune and clinical outcomes, and we will further examine the underlying mechanisms. a thorough examination of the potential clinical applications of our findings, especially their integration with immunotherapy, is needed for a more comprehensive understanding.

We performed Kaplan–Meier survival analysis across the TCGA-BLCA cohort to evaluate the prognostic significance of Senescore. Within the candidate range, we balanced sensitivity and specificity using receiver operating characteristic (ROC) curves. The final threshold

was selected to maximize the Youden index to ensure optimal discrimination of patients with distinct clinical outcomes while minimizing misclassification. The selected threshold was validated in three independent cohorts: Xiangya Cohort, IMvigor210 Cohort, and Meta-Cohort. While the current threshold demonstrates robustness, we acknowledge the need for dynamic adjustments as larger datasets emerge. Although this study provides compelling preclinical evidence, further investigation is needed to translate the Senscore-based aging scoring system into clinical practice. Prospective clinical trials are required for validation. A multi-center, randomized controlled trial is planned to further assess the accuracy and effectiveness of Senscore in predicting patient prognosis and guiding treatment decisions. Additionally, it is crucial to develop a simple, feasible, and standardized method for detecting Senscore to ensure its portability and reproducibility across diverse clinical settings.

Conclusions

Utilizing age-related and prognostically significant differentially expressed genes in BLCA, Senescence-specific molecular subtypes has been developed and validated. This quantification scoring system derived from the aging subtyping effectively characterizes the immune status, mutational landscape, and treatment predictions in BLCA.

Abbreviations

BLCA	Bladder cancer
TCGA	The cancer genome atlas
TME	Tumor microenvironment
SASP	Senescence-associated secretory phenotype
NIH	National institute of health
SEER	Surveillance, epidemiology, and end results program
DEGs	Differentially expressed genes
PCA	Principal component analysis
GO	Gene ontology
KEGG	Kyoto encyclopedia of genes and genomes
ECM	Extracellular matrix
ROC curve	Receiver operating characteristic
EGFR	Epidermal growth factor receptor
NAC	Neoadjuvant chemotherapy
GSEA	Gene set enrichment analysis
TIS	T cell-inflamed score
TMB	Tumor mutation burden
ICB	Immune checkpoint blockade
AUCs	Areas under the ROC curves
TMA	Tissue microarray
TIL	Tumor infiltrating lymphocytes
GEO	Gene expression omnibus
CNV	Copy number variation
DAA	Digital ageing atlas
PAM	Artitioning around medoids
K-M	Kaplan–Meier curve
ssGSEA	Single-sample gene set enrichment analysis
ES	Enrichment score
GSVA	Gene set variation analysis
TIICs	Tumor-infiltrating immune cells

Supplementary Information

The online version contains supplementary material available at https://doi.org/10.1186/s12885-025-13698-9.

Supplementary Material 1: Figure S1. Unsupervised clustering of TCGA-BLCA patients using Cluster_Gene_Set, related to Fig. 1. A) Cumulative distribution function for K values (2–6). B) Sample allocation in clustering status with varying K. C) Sankey plot: correlation between clusters (k = 2, k = 3, k = 4). D-I) Clustering heatmap and K-M plots for k = 2 (D-E), k = 3 (F-G), and k = 4 (H-I).

Supplementary Material 2: Figure S2. Senescore reflected the mutation landscape. A-B) Mutation profiles of top 30 genes in low Senescore group (A) and high Senescore group (B). C-D) Mutation landscape of BLCA driver genes in low (C) and high Senescore (D) group. E–F) Illustration of the differences in the landscape of RB1 (E) and TP53 (F) mutation between groups.

Supplementary Material 3: Figure S3. FGFR2/FGFR3 mutation rate in high and low Senescore groups, related to Fig. 3. A) Mutation landscape of FGFR2/FGFR3 in high Senescore group. B) Mutation landscape of FGFR2/FGFR3 in low Senescore group.

Supplementary Material 4: Figure S4. TME status for high and low Senescore groups, related to Fig. 4. A) Landscape of immunomodulators expression in Senescore and Senecluster groups. B) Heatmap showing the differential expression of SASP factors between the two Senescore and Senecluster groups. C-D) The difference of immune cell infiltration between Senescore groups (C) and Senescore clusters (D) by MCP-COUNTER. E–F) The difference of immune cell infiltration between Senescore groups (E) and Senescore clusters (F) by TIMER. G-H) The difference of anti-tumor cycle activity between Senescore groups (G) and Senescore clusters (H). The asterisks indicate a significant statistical p-value calculated using the Mann–Whitney U test (*P < 0.05; **P < 0.01; ***P < 0.001).

Supplementary Material 5: Figure S5. Correlation between the Senescore with predicted ICB response, related to Fig. 4. A) Heatmap displays the correlation between Senescore, Senecluster and TIS effector genes. B) Heatmap displays the correlation between Senescore, Senecluster and several BLCA-related signatures. C) Differential analysis of BLCA-related signatures in two Senescore groups. D) Differential analysis in enrichment of positive ICB-related signatures between two Senescore groups. The asterisks indicate a significant statistical p-value calculated using the Mann–Whitney U test (*P < 0.05; **P < 0.01; ***P < 0.001).

Supplementary Material 6: Figure S6. Oncogenic pathways differentially enriched between age and Senescore groups, and their intersection, related to Fig. 5.

Supplementary Material 7: Figure S7. Metabolic pathways differentially enriched between age and Senescore groups, and their intersection, related to Fig. 5.

Supplementary Material 8: Figure S8. Comprehensive analysis of Senescore in relation to BLCA classical molecular subtypes, immunomodulatory landscape, and immune checkpoint expression, related to Fig. 6. A) Correlation between Senescore and classical molecular subtypes. B) Heatmap of immunomodulator expression difference between Senescore groups. C) Correlation between Senescore and immune checkpoints. D-G) Linear fitting curve of the relationship between the Senescore and CD276 (D), CD274 (E), CTLA4 (F) and TIGHT (G).

Supplementary Material 9: Figure S9. TIS in different sub-Immunophenotypes, immunotherapy response, and Senescore correlations in IMvigor210 cohort, and Senescore-associated immunomodulator expression, and immune cell effector genes in meta-cohort,, related to Fig. 8. A) Linear fitting curve of the relationship between the Senescore and TIS in four sub-Immunophenotypes. B) Differences in Senescore between various TCGA phenotypes. C) relationship between immunoefficacy and Senescore in three immunophenotypes. D) Heatmap of key immune cell effector gene expression difference between Senescore groups. E) Heatmap of immunomodulator expression difference between Senescore groups. The asterisks indicate a significant statistical p-value calculated using the Mann–Whitney U test (*P < 0.05; **P < 0.01; ***P < 0.001).

Supplementary Material 10: Table S1. Raw_Gene_Set. Specific genes contained in the Raw_Gene_Set.

Supplementary Material 11: Table S2. Cluster_Gene_Set. Specific genes contained in the Cluster_Gene_Set.

Supplementary Material 12: Table S3. Score construction. Composition Information of Senescore Establishment.

Supplementary Material 13: Table S4. Oncogentic pathways bwtween Onco_score and Onco_age.

Supplementary Material 14: Table S5. Hallmark pathways of Hallmark_ score and Hallmark_age.

Acknowledgements
We acknowledge all authors participating in this study for data collection, preparation, and quality control.

Authors' contributions
Conception and design: Zu X, Hu J, and Dai Y. Acquisition of data: Hu J, Liang H, Yan L, Fan B, Qi T, Liu J, He Y, Chen M, Yao Y, Wang K and Deng D. Analysis and interpretation of data: Hu J, Yan L, Liang H, Deng D, Liu J and Qi T. Drafting of the manuscript: Yan L, Liang H, Deng D, Liu J, He Y, Yao Y, Wang K, and Qi T. Critical revision of the manuscript for important intellectual content: Yan L, Liang H, Deng D, Liu J, Hu J, Chen J and Qi T. Statistical analysis: Yan L, Liang H, Deng D, Liu J and Qi T. Obtaining funding: Hu J, Zu X and Fan B. Administrative, technical, or material support: Hu J, Zu X Chen M, Fan B and Dai Y. Supervision: Hu J, Zu X and Dai Y.

Funding
This work was supported by the National Natural Science Foundation of China (82303760, 82373337, 82070785), the China Postdoctoral Innovation Talents Support Program (BX20230431), the China Postdoctoral Science Foundation (2023M733951), Hunan Natural Science Foundation (2023JJ40946, 2024JJ2093), Hunan Provincial Key Area Research Plan (2023SK2016), Hunan Province Young Talents Program (2023RC3073, 2021RC3027), Changsha Natural Science Foundation (kq2208377), and the Youth Science Foundation of Xiangya Hospital (2022Q20).

Data availability
All data generated from this study are available upon request to the corresponding author.

Declarations

Ethics approval and consent to participate
In accordance with the Declaration of Helsinki, the study plan was approved by the ethics committee of Xiangya Hospital, Central South University. All the specimens were collected complying with informed consent right.

Consent for publication
Not applicable.

Competing interests
The authors declare no competing interests.

Author details
[1]Department of Urology, Xiangya Hospital, Central South University, Changsha, Hunan 410008, China. [2]National Clinical Research Center for Geriatric Disorders, Xiangya Hospital, Central South University, Changsha, Hunan, China. [3]Hunan Province Bladder Preservation Treatment Consortium, Changsha, Hunan, China. [4]XiangYa School of Medicine, Central South University, Changsha, Hunan, China. [5]Furong Laboratory, Changsha, Hunan, China. [6]Department of Urology, Hunan Provincial People's Hospital, the First Affiliated Hospital of Hunan Normal University, Changsha, Hunan, China.

Received: 30 December 2024 Accepted: 10 February 2025
Published online: 19 February 2025

References

1. Dyrskjøt L, Hansel DE, Efstathiou JA, Knowles MA, Galsky MD, Teoh J, et al. Bladder cancer. Nat Rev Dis Primers. 2023;9(1):58.
2. Meeks JJ, Al-Ahmadie H, Faltas BM, Taylor JA 3rd, Flaig TW, DeGraff DJ, et al. Genomic heterogeneity in bladder cancer: challenges and possible solutions to improve outcomes. Nat Rev Urol. 2020;17(5):259–70.
3. Tran L, Xiao JF, Agarwal N, Duex JE, Theodorescu D. Advances in bladder cancer biology and therapy. Nat Rev Cancer. 2021;21(2):104–21.
4. Felsenstein KM, Theodorescu D. Precision medicine for urothelial bladder cancer: update on tumour genomics and immunotherapy. Nat Rev Urol. 2017;15(2):92–111.
5. McGranahan N, Swanton C. Clonal heterogeneity and tumor evolution: past, present, and the future. Cell. 2017;168(4):613–28.
6. Shariat SF, Sfakianos JP, Droller MJ, Karakiewicz PI, Meryn S, Bochner BH. The effect of age and gender on bladder cancer: a critical review of the literature. BJU Int. 2010;105(3):300–8.
7. Martin A, Woolbright BL, Umar S, Ingersoll MA, Taylor JA. Bladder cancer, inflammageing and microbiomes. Nat Rev Urol. 2022;19(8):495–509.
8. Li CH, Haider S, Boutros PC. Age influences on the molecular presentation of tumours. Nature Commun. 2022;13(1):208.
9. Wang X, Langevin A-M, Houghton PJ, Zheng S. Genomic disparities between cancers in adolescent and young adults and in older adults. Nat Commun. 2022;13(1):7223.
10. López-Otín C, Pietrocola F, Roiz-Valle D, Galluzzi L, Kroemer G. Meta-hallmarks of aging and cancer. Cell Metab. 2023;35(1):12–35.
11. Aunan JR, Cho WC, Søreide K. The biology of aging and cancer: a brief overview of shared and divergent molecular hallmarks. Aging Dis. 2017;8(5):628–42.
12. Fane M, Weeraratna AT. How the ageing microenvironment influences tumour progression. Nat Rev Cancer. 2019;20(2):89–106.
13. Gabai Y, Assouline B, Ben-Porath I. Senescent stromal cells: roles in the tumor microenvironment. Trends in Cancer. 2023;9(1):28–41.
14. Faget DV, Ren Q, Stewart SA. Unmasking senescence: context-dependent effects of SASP in cancer. Nat Rev Cancer. 2019;19(8):439–53.
15. Gui C, Wei J, Mo C, Liang Y, Cen J, Chen Y, Wang D, Luo J. Therapeutic implications for localized prostate cancer by multiomics analyses of the ageing microenvironment landscape. Int J Biol Sci. 2023;19(12):3951–69.
16. Liu S, Meng Y, Zhang Y, Qiu L, Wan X, Yang X, Zhang Y, Liu X, Wen L, Lei X, et al. Integrative analysis of senescence-related genes identifies robust prognostic clusters with distinct features in hepatocellular carcinoma. J Adv Res. 2024;04:007.
17. Meguro S, Johmura Y, Wang TW, Kawakami S, Tanimoto S, Omori S, Okamura YT, Hoshi S, Kayama E, Yamaguchi K, et al. Preexisting senescent fibroblasts in the aged bladder create a tumor-permissive niche through CXCL12 secretion. Nature aging. 2024;4(11):1582–97.
18. Sheng X, Yan X, Wang L, Shi Y, Yao X, Luo H, et al. Open-label, Multicenter, Phase II Study of RC48-ADC, a HER2-targeting antibody-drug conjugate, in patients with locally advanced or metastatic urothelial carcinoma. Clin Cancer Res. 2021;27(1):43–51.
19. Li H, Chen J, Li Z, Chen M, Ou Z, Mo M, et al. S100A5 Attenuates Efficiency of Anti-PD-L1/PD-1 Immunotherapy by Inhibiting CD8(+) T Cell-Mediated Anti-Cancer Immunity in Bladder Carcinoma. Adv Sci (Weinh). 2023;10(25): e2300110.
20. Hu J, Othmane B, Yu A, Li H, Cai Z, Chen X, et al. 5mC regulator-mediated molecular subtypes depict the hallmarks of the tumor microenvironment and guide precision medicine in bladder cancer. BMC Med. 2021;19(1):289.
21. Cai Z, Chen J, Yu Z, Li H, Liu Z, Deng D, et al. BCAT2 Shapes a Noninflamed Tumor Microenvironment and Induces Resistance to Anti-PD-1/PD-L1 Immunotherapy by Negatively Regulating Proinflammatory Chemokines and Anticancer Immunity. Adv Sci (Weinh). 2023;10(8):e2207155.
22. Liu Z, Qi T, Li X, Yao Y, Othmane B, Chen J, et al. A Novel TGF-β risk score predicts the clinical outcomes and tumour microenvironment phenotypes in bladder cancer. Front Immunol. 2021;12:791924.
23. Yu A, Hu J, Fu L, Huang G, Deng D, Zhang M, et al. Bladder cancer intrinsic LRFN2 drives anticancer immunotherapy resistance by attenuating CD8(+) T cell infiltration and functional transition. J Immunother Cancer. 2023;11(10):e007230.
24. Hu J, Yu A, Othmane B, Qiu D, Li H, Li C, et al. Siglec15 shapes a non-inflamed tumor microenvironment and predicts the molecular subtype in bladder cancer. Theranostics. 2021;11(7):3089–108.

25. Mermel CH, Schumacher SE, Hill B, Meyerson ML, Beroukhim R, Getz G. GISTIC2.0 facilitates sensitive and confident localization of the targets of focal somatic copy-number alteration in human cancers. Genome Biol. 2011;12(4):R41.
26. Balar AV, Galsky MD, Rosenberg JE, Powles T, Petrylak DP, Bellmunt J, et al. Atezolizumab as first-line treatment in cisplatin-ineligible patients with locally advanced and metastatic urothelial carcinoma: a single-arm, multicentre, phase 2 trial. Lancet. 2017;389(10064):67–76.
27. Mariathasan S, Turley SJ, Nickles D, Castiglioni A, Yuen K, Wang Y, et al. TGFβ attenuates tumour response to PD-L1 blockade by contributing to exclusion of T cells. Nature. 2018;554(7693):544–8.
28. Choi W, Porten S, Kim S, Willis D, Plimack ER, Hoffman-Censits J, et al. Identification of distinct basal and luminal subtypes of muscle-invasive bladder cancer with different sensitivities to frontline chemotherapy. Cancer Cell. 2014;25(2):152–65.
29. Sjödahl G, Lauss M, Lövgren K, Chebil G, Gudjonsson S, Veerla S, et al. A molecular taxonomy for urothelial carcinoma. Clin Cancer Res. 2012;18(12):3377–86.
30. de Magalhães JP, Toussaint O. GenAge: a genomic and proteomic network map of human ageing. FEBS Lett. 2004;571(1–3):243–7.
31. Rafikova E, Nemirovich-Danchenko N, Ogmen A, Parfenenkova A, Velikanova A, Tikhonov S, et al. Open Genes-a new comprehensive database of human genes associated with aging and longevity. Nucleic Acids Res. 2023;52(D1):D950–62.
32. Avelar RA, Ortega JG, Tacutu R, Tyler EJ, Bennett D, Binetti P, et al. A multidimensional systems biology analysis of cellular senescence in aging and disease. Genome Biol. 2020;21(1):91.
33. Huang K, Gong H, Guan J, Zhang L, Hu C, Zhao W, et al. AgeAnno: a knowledgebase of single-cell annotation of aging in human. Nucleic Acids Res. 2023;51(D1):D805–15.
34. Saul D, Kosinsky RL, Atkinson EJ, Doolittle ML, Zhang X, LeBrasseur NK, et al. A new gene set identifies senescent cells and predicts senescence-associated pathways across tissues. Nat Commun. 2022;13(1):4827.
35. Robertson AG, Kim J, Al-Ahmadie H, Bellmunt J, Guo G, Cherniack AD, et al. Comprehensive Molecular Characterization of Muscle-Invasive Bladder Cancer. Cell. 2018;174(4):1033.
36. Rebouissou S, Bernard-Pierrot I, de Reyniès A, Lepage ML, Krucker C, Chapeaublanc E, et al. EGFR as a potential therapeutic target for a subset of muscle-invasive bladder cancers presenting a basal-like phenotype. Sci Transl Med. 2014;6(244):244ra91.
37. Damrauer JS, Hoadley KA, Chism DD, Fan C, Tiganelli CJ, Wobker SE, et al. Intrinsic subtypes of high-grade bladder cancer reflect the hallmarks of breast cancer biology. Proc Natl Acad Sci U S A. 2014;111(8):3110–5.
38. Mo Q, Nikolos F, Chen F, Tramel Z, Lee YC, Hayashi K, et al. Prognostic power of a tumor differentiation gene signature for bladder urothelial carcinomas. J Natl Cancer Inst. 2018;110(5):448–59.
39. Kamoun A, de Reynies A, Allory Y, Sjodahl G, Robertson AG, Seiler R, et al. A Consensus Molecular Classification of Muscle-invasive Bladder Cancer. Eur Urol. 2020;77(4):420–33.
40. Xu L, Deng C, Pang B, Zhang X, Liu W, Liao G, et al. TIP: A web server for resolving tumor immunophenotype profiling. Can Res. 2018;78(23):6575–80.
41. Motterle G, Andrews JR, Morlacco A, Karnes RJ. Predicting response to neoadjuvant chemotherapy in bladder cancer. Eur Urol Focus. 2020;6(4):642–9.
42. Siefker-Radtke AO, Necchi A, Park SH, García-Donas J, Huddart RA, Burgess EF, et al. Efficacy and safety of erdafitinib in patients with locally advanced or metastatic urothelial carcinoma: long-term follow-up of a phase 2 study. Lancet Oncol. 2022;23(2):248–58.
43. Loriot Y, Necchi A, Park SH, Garcia-Donas J, Huddart R, Burgess E, et al. Erdafitinib in locally advanced or metastatic urothelial carcinoma. N Engl J Med. 2019;381(4):338–48.
44. Loriot Y, Matsubara N, Park SH, Huddart RA, Burgess EF, Houede N, et al. Erdafitinib or chemotherapy in advanced or metastatic urothelial carcinoma. N Engl J Med. 2023;389(21):1961–71.
45. Ayers M, Lunceford J, Nebozhyn M, Murphy E, Loboda A, Kaufman DR, et al. IFN-γ-related mRNA profile predicts clinical response to PD-1 blockade. J Clin Invest. 2017;127(8):2930–40.
46. Liu W, Shen D, Ju L, Zhang R, Du W, Jin W, et al. MYBL2 promotes proliferation and metastasis of bladder cancer through transactivation of CDCA3. Oncogene. 2022;41(41):4606–17.
47. Zhou Z, Zhang Z, Chen H, Bao W, Kuang X, Zhou P, et al. SBSN drives bladder cancer metastasis via EGFR/SRC/STAT3 signalling. Br J Cancer. 2022;127(2):211–22.
48. Wang C, Liu Q, Huang M, Zhou Q, Zhang X, Zhang J, et al. Loss of GATA6 expression promotes lymphatic metastasis in bladder cancer. Faseb j. 2020;34(4):5754–66.
49. Zhang Q, Qi T, Long Y, Li X, Yao Y, Wu Q, et al. GATA3 Predicts the tumor microenvironment phenotypes and molecular subtypes for bladder carcinoma. Front Surg. 2022;9:860663.
50. Yeh HC, Huang CN, Li CC, Chang LL, Lin HH, Ke HL, et al. Overexpression of PTP4A3 is associated with metastasis and unfavorable prognosis in bladder cancer. World J Urol. 2016;34(6):835–46.
51. Zhang L, Li Y, Zhou L, Zhou H, Ye L, Ou T, et al. The m6A Reader YTHDF2 Promotes Bladder Cancer Progression by Suppressing RIG-I-Mediated Immune Response. Cancer Res. 2023;83(11):1834–50.
52. Chen H, Yang W, Li Y, Ji Z. PLAGL2 promotes bladder cancer progression via RACGAP1/RhoA GTPase/YAP1 signaling. Cell Death Dis. 2023;14(7):433.
53. Lu S, Guo M, Fan Z, Chen Y, Shi X, Gu C, et al. Elevated TRIP13 drives cell proliferation and drug resistance in bladder cancer. Am J Transl Res. 2019;11(7):4397–410.
54. Gorgoulis V, Adams PD, Alimonti A, Bennett DC, Bischof O, Bishop C, et al. Cellular Senescence: Defining a Path Forward. Cell. 2019;179(4):813–27.
55. Grigorash BB, van Essen D, Liang G, Grosse L, Emelyanov A, Kang Z, et al. p16High senescence restricts cellular plasticity during somatic cell reprogramming. Nat Cell Biol. 2023;25(9):1265–78.
56. Győrffy B. Transcriptome-level discovery of survival-associated biomarkers and therapy targets in non-small-cell lung cancer. Br J Pharmacol. 2024;181(3):362–74.
57. Giusti R, Mazzotta M, Filetti M, Marinelli D, Di Napoli A, Scarpino S, et al. CDKN2A/B gene loss and MDM2 alteration as a potential molecular signature for hyperprogressive disease in advanced NSCLC: A next-generation-sequencing approach. Am Soc Clin Oncol; 2019;37(15).

Publisher's Note